

EXPERIMENTAL VERIFICATION AND PRACTICAL APPLICATION
OF TORQUEWHIRL THEORY OF ROTORDYNAMIC INSTABILITY

J.M. Vance and S.T. Noah
Texas A&M University
College Station, Texas 77843

K.B. Yim
Sunstrand Aviation
Rockford, Illinois

A theory developed by the first author in 1978 to explain the destabilizing effect of torque on a whirling rotor has been experimentally verified. The measurements made on a specially designed test apparatus are described.

New computer models have also been developed to investigate the effect of torque on rotordynamic stability of multi-disk flexible rotor-bearing systems. The effect of torque has been found to be most pronounced when the system is already marginally stable from other influences. The modifications required to include torque in a typical shaft transfer matrix are described, and results are shown which identify the type of rotor design most sensitive to load torque.

INTRODUCTION

Since at least the early 1950's, it has been known that large values of load torque can depress the natural frequencies of a uniform shaft on short or long bearings [1,2,3], and that any value of torque on a cantilevered shaft, without damping, produces dynamic instability [4,5,6,7]. These results have limited application to most rotating machinery, however, since the values of torque required to depress critical speeds are seldom approached and all real machines have at least some amount of damping. Although the effect of torque on critical speeds is mostly of academic interest, recent experimental and analytical investigations by the authors have shown that the effect on whirl stability, with damping included, for some rotor-bearing configurations which are representative of contemporary machines, can be significant. In 1978 the first author published a nonlinear analysis with damping included [8] which showed that tangential load torque on a rotor disk (e.g., the stage torque on a fluid impeller) can produce nonsynchronous whirling with amplitude dependent on the ratio of torque to damping.

Figure 1 shows the model analyzed in reference [8] where all of the rotor flexibility was concentrated in the joint at 0' (the shaft was assumed rigid). This is the simplest possible model which can demonstrate the torquewhirl phenomenon, as considerations of the effect of the torque on the shaft deflection mode shape are avoided.

Subsequently, Tison [9] linearized the equations of motion for the same model and applied the Routh-Hurwitz criteria to obtain the required condition for whirl stability, which is

$$\frac{T}{C_t \omega_d l^2} < 2 \quad (1)$$

where C_t is the translational viscous coefficient of damping acting at the disk and ω_d is the whirling frequency.

More recently, Yim [10] has extended the torquewhirl analysis to more realistic rotor models, including the disk cantilevered on an elastic shaft (Figure 2), and even to generalized multi-disk rotors using the transfer matrix method.

An experimental program has also been conducted [10] to verify the existence of nonsynchronous whirl produced exclusively by tangential load torque.

The purpose of this paper is to present the main results of the experimental program and to condense the useful results of the recent analyses (since reference 9) which are relevant to practical applications in rotor-dynamics. The work reported here was supported by the National Science Foundation, Grant #MEA-8115330.

EXPERIMENTAL VERIFICATION

Apparatus and Instrumentation

To facilitate isolation of the torquewhirl effect, a special test rig was designed to represent the model of Figure 1. The test rig design concept was by Professor George N. Sandor at the University of Florida. This is the simplest possible rotor configuration capable of demonstrating the torquewhirl phenomenon. In particular, there is only one mode of whirling (conical), and the torque has no effect on the mode shape. Also, an exact solution to the nonlinear equations of motion was available for this model [8], which extended the opportunities for comparison with theory.

Figures 3 and 4 are a photograph and schematic, respectively, of the test rig hardware. From left to right there is a 15 KW variable speed electric motor, driving through a toothed belt speed reducer, and the rotor which is mounted on ball bearings (vertical axis) inside a finned housing. The purpose of the housing is to apply a load torque to the rotor which always remains aligned with the rotor axis, even while whirling occurs. Thus the housing precesses with the rotor in its conical whirl mode, but is restrained from spinning by the four springs. The springs are radially oriented while the system is at rest. In operation, torque rotates the housing through an angle until an equilibrium of moments is reached.

Figure 5 shows a cross section of the rotor and housing. Torque is applied to the rotor by viscous shear in the conical clearance space when it is filled with a silicone fluid. The clearance is adjustable by a threaded collar which moves the housing up or down relative to the rotor.

The flexible joint (O' in Figure 1) is provided in the test rig by a laminated disk coupling on the shaft just above the housing. The forward natural frequency of the test rig at 1000 rpm was calculated to be 10.78 Hz, and turned out to be about 10.5 Hz.

During the testing, the drag cylinder attached to the bottom of the housing was immersed to a controlled depth in oil, so that the damping of the whirl motion

was adjustable. Three different values of damping, as determined by measurements of the logarithmic decrement of free vibration, were used in the test program: 2.2%, 3.8%, and 5.2% of the critical value.

Two proximity probes are installed near the upper part of the drag cylinder for measurement of the whirl orbit (x-y vibration displacement signals). Rotor speed (0-1200 rpm) is measured with a digital tachometer excited once per revolution from the shaft by a fiberoptic transducer with reflective tape. A strain gage mounted on one of the spring restraining brackets was calibrated to measure the rotor torque.

All signals were electronically converted from analog to digital form for plotting by a desktop computer. The x-y vibration signals were filtered with a bandpass range of 18%, for measurement of the 10.5 Hz whirl frequency. Both the filtered and unfiltered signals were recorded and plotted. Calibration procedures are described in reference [10].

The variable parameters in the test program were speed, external damping, and to a lesser extent, torque. A factor which limited the time duration of each test was heating of the rotor and housing from viscous shear, in spite of the cooling fins on the housing and forced air cooling with a Hilsch tube.

Experimental Results

Figure 6 shows measured data for speed, torque, and whirl amplitude, plotted in the time domain with no load torque (air in the clearance space). Figure 7 shows the frequency spectrum of the unfiltered vibration signal (whirl amplitude). The two components are synchronous whirl (from rotor unbalance and misalignment) and subsynchronous whirl excited by the drive belt. The latter vibration was found to track at a frequency of exactly .56 times rotor speed, which is the ratio of teeth on the large pulley to teeth on the belt.

Figures 6 and 7 were obtained with the drag cylinder immersed to a depth which gives 2.2% of critical damping. This was found to be the minimum damping required to suppress subsynchronous whirl produced by internal friction in the laminated disk coupling. The internal friction effect was explored experimentally [10] and found to be independent of torque.

Figures 8 and 9 show the same measurements made with load torque applied (silicone fluid in the clearance space). Note the large increase in whirl amplitude (Figure 8), which is seen to be largely subsynchronous at the predicted torqu whirl frequency (Figure 9). Figures 10 and 11 show similar results with increased external damping (5.2%).

A nonlinear relationship between applied torque and whirl amplitude was observed. Figure 12 shows the whirl amplitude decreasing as the torque (and speed) are increasing above the initial destabilizing value. This phenomenon is explained by a nonlinear analysis presented in reference [10]. It cannot be predicted or simulated by a linearized stability analysis.

PRACTICAL APPLICATIONS

Effect of Rotor Configuration and Geometry

Rotordynamic stability analyses have been conducted to evaluate the effect of tangential load torque on a wide variety of rotor configurations. Several different methods were used to determine the eigenvalues, including flexibility influence coefficients, the transfer matrix, and the Galerkin method [10,11], with excellent agreement of results.

The destabilizing effect of torque on rotor whirl has been found to be most pronounced on overhung (cantilevered) rotors, and in rotors with a high ratio of torque to bending stiffness (TL/EI). There is, however, a strength of materials limitation on this latter ratio. To illustrate, Figure 13 shows that $TL/EI < 0.5$ for uniform shafts of typical L/D and for typical steels of shear strength τ .

Besides the value of TL/EI , the mode shape is the most important factor in determining the sensitivity of a rotor to torquewhirl. The mode shape determines the misalignment of the tangential torque vectors applied at different axial locations along the rotor, and also has a large influence on another important factor, the ratio of torque to damping. The mode shape determines the effectiveness of bearing damping, since bearings located near nodal points can make little contribution to the system damping.

The sense of the torques (positive or negative) relative to the direction of shaft speed determines the direction of whirl. For a cantilevered rotor with load torque applied along the axis of the overhung disk, positive torque (e.g., a turbine) produces backward whirl, and negative torque (e.g., a compressor) produces forward whirl (provided the ratio of torque to damping is high enough).

For a multi-disk rotor, the situation is similar, but more complex. Figure 14 shows the mode shapes for two different configurations, each with two disks. Configuration A has both disks inboard of the bearings, while configuration B has one of the disks overhung.

Figure 15 shows the effect of torque on the stability of the four natural whirl frequencies. Damping is omitted and $TL/EI > 1$ to maximize the torque-whirl effect. In each case, one disk is a driver (e.g., turbine) and the other is a load (e.g., compressor). Case B has the load torque on the overhung wheel.

Without torque, both cases (A1, B1) have zero logarithmic decrements as expected. With torque, the logarithmic decrement of case A2 is little changed, but case B2 is destabilized in forward whirl (F) and stabilized in backward whirl (B). The opposite torques have a cancelling effect on the symmetric rotor A, but destabilize case B due to the unsymmetric mode shape.

A torquewhirl analysis of several existing turbomachines has been conducted. In most cases torque was found to be a second order effect when compared to the destabilizing influences from fluid-film bearings, seals, and Alford-type forces [12]. Two examples of the machines analyzed are an eight-stage centrifugal compressor [13], and the High Pressure Oxygen Turbopump used in the NASA Space Shuttle engine [10,14].

There are, however, potential exceptions such as the single-stage overhung

centrifugal compressor illustrated in Figure 16. This machine is representative of the general type described in reference [15]. Although the numerical values used in the rotordynamic model were approximated by scaling a drawing, they are believed to be realistic. In this case it was found that at least 12% of critical damping is required to suppress rotordynamic instability from load torque alone.

Whirl instabilities in turbomachines are often caused by several destabilizing influences acting in concert [12], so the torquewhirl effect should be added in any case to improve the accuracy of predicted threshold speeds and loads. The studies referenced here have shown the torquewhirl effect to be much more pronounced on a system which is already unstable than on an otherwise stable system. This helps to explain why marginally stable turbomachines have been observed to be very sensitive to the load.

Computer Modeling of Torque Effects

Most computer programs for rotordynamic stability analysis are based on the transfer matrix method [13,16], while others use a characteristic matrix [17] based on either stiffness or flexibility elements to model the elastic shaft forces and moments.

The flexibility matrix approach with torque effects included is illustrated in a companion by the authors [11] and in reference [10].

The transfer matrix for a shaft section, or elastic element of the nth "station", with torque included is given by

$$\begin{Bmatrix} x \\ y \\ \alpha \\ \beta \\ v_x \\ v_y \\ M_x \\ M_y \end{Bmatrix}_{n+1} = \begin{bmatrix} 1 & 0 & l & 0 & C_{11} & C_{12} & C_{13} & C_{14} \\ 0 & 1 & 0 & l & C_{21} & C_{22} & C_{23} & C_{24} \\ 0 & 0 & 1 & 0 & C_{31} & C_{32} & C_{33} & C_{34} \\ 0 & 0 & 0 & 1 & C_{41} & C_{42} & C_{43} & C_{44} \\ 0 & 0 & 0 & 0 & 1 & 0 & 0 & 0 \\ 0 & 0 & 0 & 0 & 0 & 1 & 0 & 0 \\ 0 & 0 & 0 & 0 & C_{51} & C_{52} & C_{53} & C_{54} \\ 0 & 0 & 0 & 0 & C_{61} & C_{62} & C_{63} & C_{64} \end{bmatrix} \begin{Bmatrix} x \\ y \\ \alpha \\ \beta \\ v_x \\ v_y \\ M_x \\ M_y \end{Bmatrix}_n \tag{2}$$

where the state variables are defined by Figure 17 and the C_{ij} are as follows:

$$\begin{aligned}
C_{11} &= C_{22} = \xi(l - \xi T \sin \gamma) \\
C_{12} &= -C_{21} = \xi^2 T(1 - \cos \gamma) - \frac{l^2}{2T} \\
C_{13} &= C_{24} = C_{31} = C_{42} = \xi(1 - \cos \gamma) \\
C_{14} &= -C_{23} = C_{32} = -C_{41} = \xi \sin \gamma - \frac{l}{T} \\
C_{33} &= C_{44} = \left(\frac{1}{T}\right) \sin \gamma \\
C_{34} &= -C_{43} = \left(\frac{1}{T}\right)(\cos \gamma - 1) \\
C_{51} &= C_{62} = \xi T \sin \gamma \\
C_{52} &= -C_{61} = \xi T(\cos \gamma - 1) \\
C_{53} &= C_{64} = \cos \gamma \\
C_{54} &= -C_{63} = -\sin \gamma
\end{aligned} \tag{3}$$

where $\xi = EI/T^2$ and $\gamma = Tl/EI$.

In more compact form, Eq. (2) becomes

$$\{X\}_{n+1}^L = [T_s]_n \{X\}_n^R \tag{4}$$

where

$\{X\}_{n+1}^L$ = state vector on the left side of station $n + 1$

$\{X\}_n^R$ = state vector on the right side of station n

$[T_s]$ = transfer matrix for the shaft section between

Conclusions

The destabilizing effect of load torque on a rotating machine, to produce non-synchronous whirl, has been demonstrated experimentally.

Analytical studies have shown that whirl instability due to torque alone requires a high ratio of torque to damping and a whirling mode shape which misaligns the driving and driven torque vectors with respect to each other. This combination of conditions are usually not obtained in most contemporary turbo-machines, but load torque can have a significant effect when combined with other destabilizing mechanisms. The type of machine most sensitive to torque-whirl was found to be the single-overhung wheel on a flexible shaft with negative work load (i.e., compressor).

The destabilizing effect of torque can be incorporated into the shaft transfer matrices used in most contemporary computer programs for rotordynamic stability analysis, but a nonlinear analysis is required to explain the effect of torque which exceeds the threshold value.

REFERENCES

1. Golomb, M., and Rosenberg, R. M., "Critical Speeds of Uniform Shafts Under Axial Torque," Proceedings of The U.S. National Congress on Applied Mechanics, New York, 1951, pp. 103-110.
2. Eshleman, R. L., and Eubanks, R. A., "On the Critical Speed of a Continuous Rotor," ASME Journal of Engineering for Industry, Nov. 1969, pp. 1180-1188.
3. Biezeno, C. B., and Grammel, R., Engineering Dynamics, Volume III, London, 1954.
4. Ziegler, H., Principles of Structural Stability, Blaisdell Publishing Company, London, 1968.
5. Nikolai, E. L., "On the Stability of the Rectilinear Form of a Compressed and Twisted Bar (in Russian)," Izvest. Leningr. Politekhn. in-ta 31, 1928.
6. Morris, J., "Torque and the Flexural Stability of a Cantilever," Aircraft Engineering, Vol. 23, 1951, pp. 375-377.
7. Shieh, R. C., "Some Principles of Elastic Shaft Stability Including Variational Principles," ASME Journal of Applied Mechanics, March 1982, pp. 191-196.
8. Vance, J. M., "Torquewhirl - A Theory to Explain NonSynchronous Whirling Failure of Rotors with High Load Torque," ASME Journal of Engineering for Power, Apr. 1978, pp. 235-240.
9. Tison, J. D., Dynamic Stability Analysis of Overhung Rotors with High Load Torque, Master of Engineering Thesis in Mechanical Engineering, University of Florida, 1977.
10. Yim, K. B., Load-Induced Rotordynamic Instabilities in Turbomachinery, Ph.D. Dissertation in Mechanical Engineering, Texas A&M University, December 1984.
11. Yim, K. B., Noah, S. T., and Vance, J. M., "Effect of Tangential Torque on the Dynamics of Flexible Rotors," to be published, 1985.
12. Vance, J. M., "Instabilities on Turbomachinery," Proceedings of the 5th Annual Seminar on Machinery Vibration Analysis, The Vibration Institute, New Orleans, La., April 7-9, 1981.
13. Lund, J. W., "Stability and Damped Critical Speeds of a Flexible Rotor in Fluid-Film Bearings," ASME Journal of Engineering for Industry, May 1974, pp. 509-517.
14. Childs, D., and Moyer, D., "Vibration Characteristics of the HPOTP of the SSME," ASME Journal of Engineering for Gas Turbine and Power, pp. 152-159, Vol. 107, ASME Transactions, January 1985.

15. Pennink, H., "The State of the Art of High Speed Overhung Centrifugal Compressors for the Process Industry," proceedings of the Seventh Turbomachinery Symposium, Texas A&M University, Dec. 1978, pp. 35-46.
16. Murphy, B. T., and Vance, J. M., "An Improved Method for Calculating Critical Speeds and Rotordynamic Stability of Turbomachinery," ASME Journal of Engineering for Power, Vol. 103, July 1983, pp. 591-595.
17. Thomson, W. T., Theory of Vibration With Applications, 2nd Edition, Prentice-Hall, Inc., Englewood Cliffs, New Jersey, 1981, pp. 174-184.

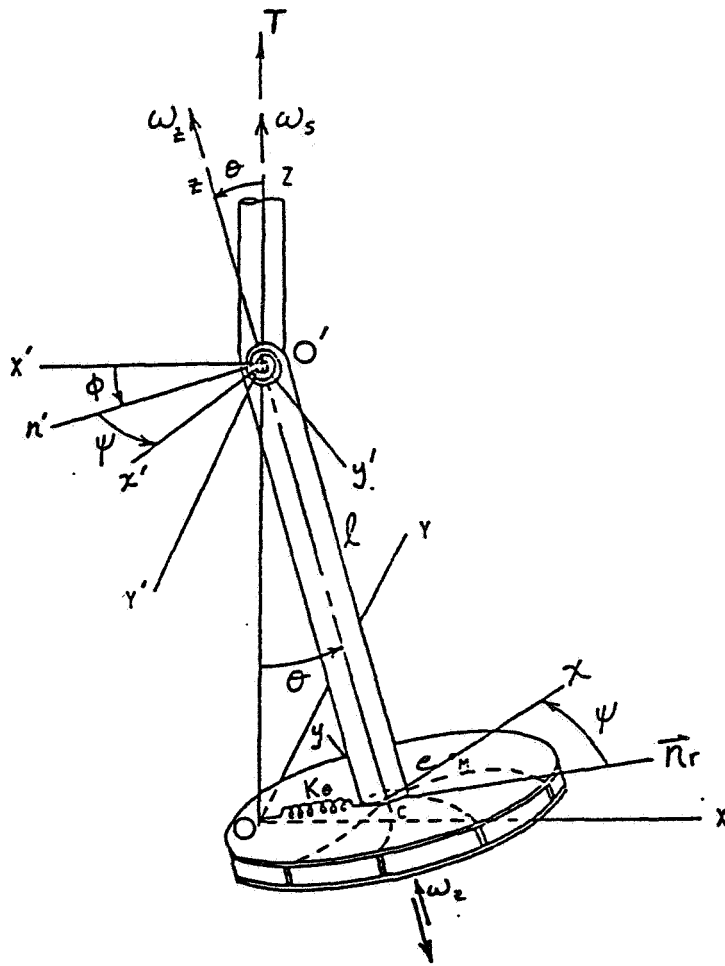


Figure 1. - Rigid-shaft model from Reference [8].

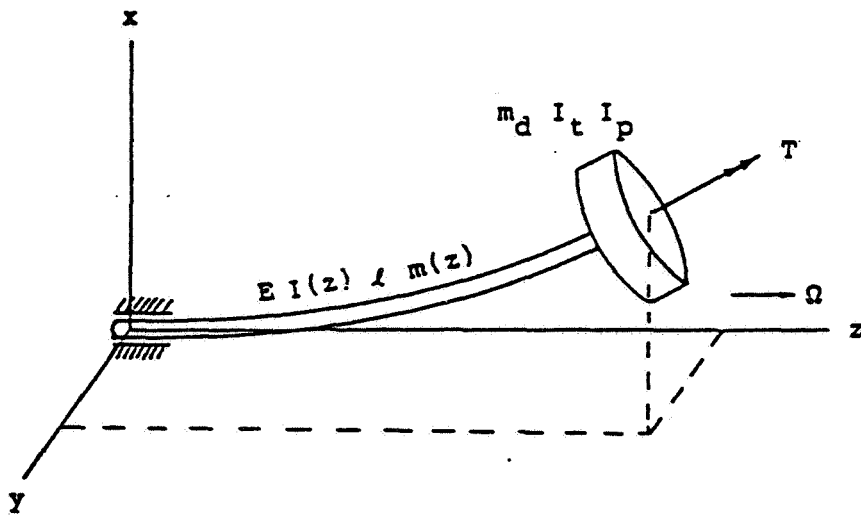


Figure 2. - Cantilevered rotor with flexible shaft.

ORIGINAL PAGE IS
OF POOR QUALITY

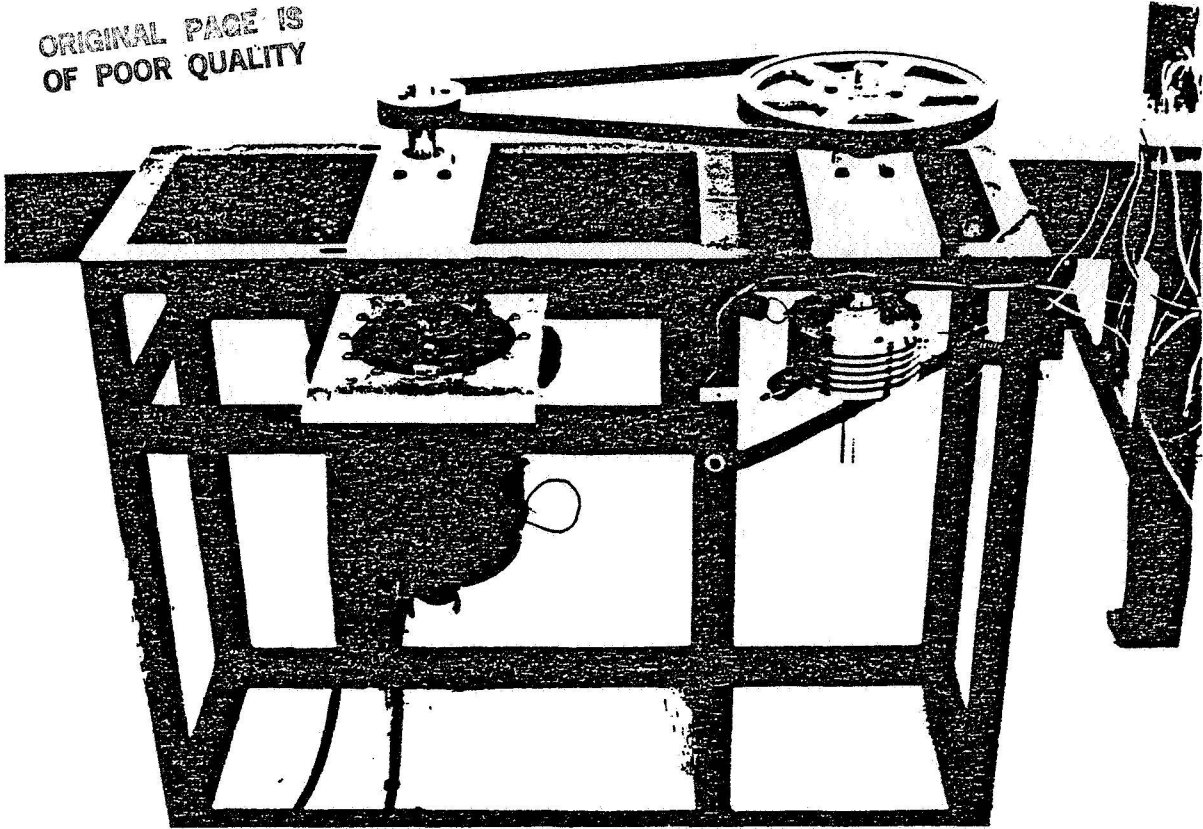


Figure 3. - Test rig.

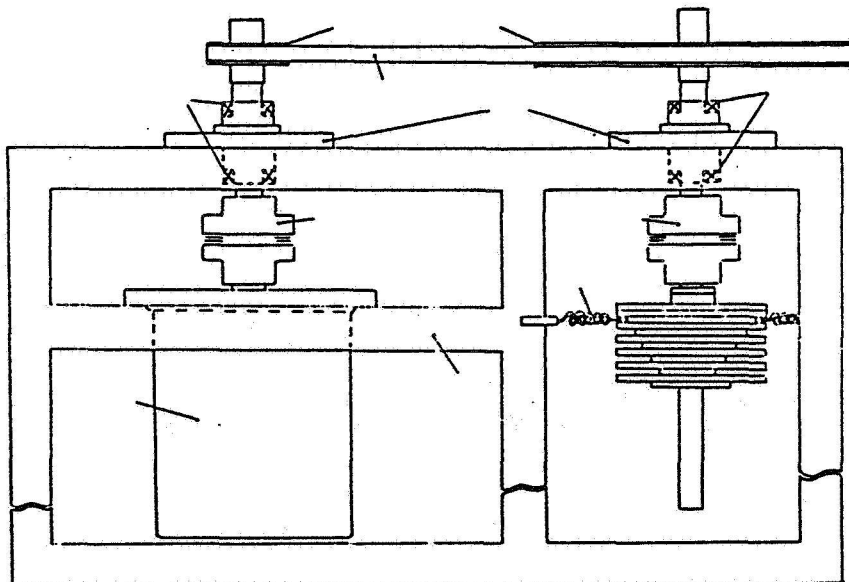


Figure 4. - Sketch of test rig.

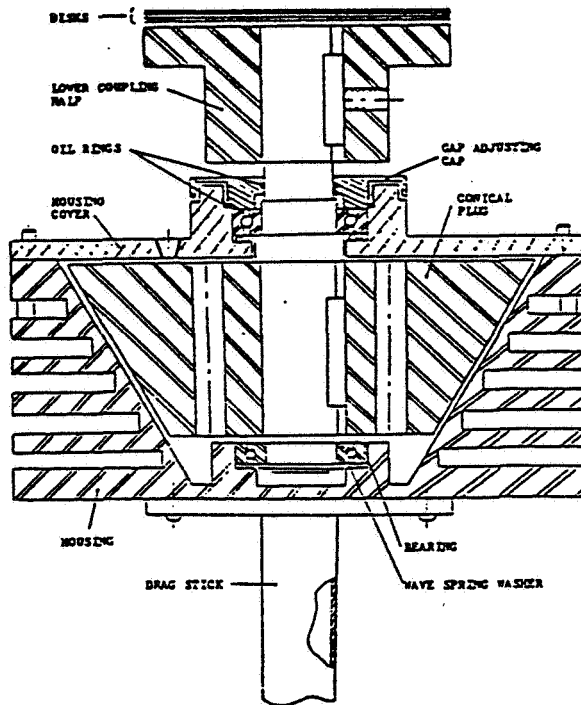


Figure 5. - Cross section of housing.

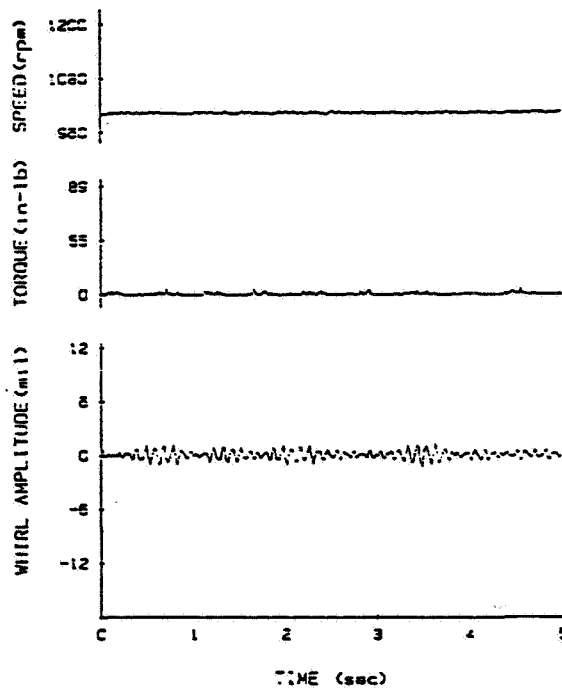


Figure 6. - Time domain data without load torque (2.2 percent damping; 1000 rpm).

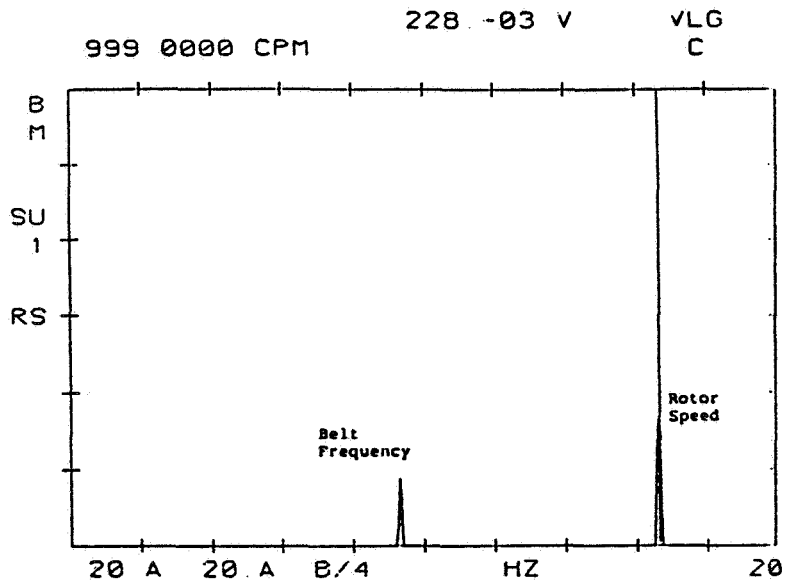


Figure 7. - Frequency domain data without load torque (2.2 percent damping; 1000 rpm).

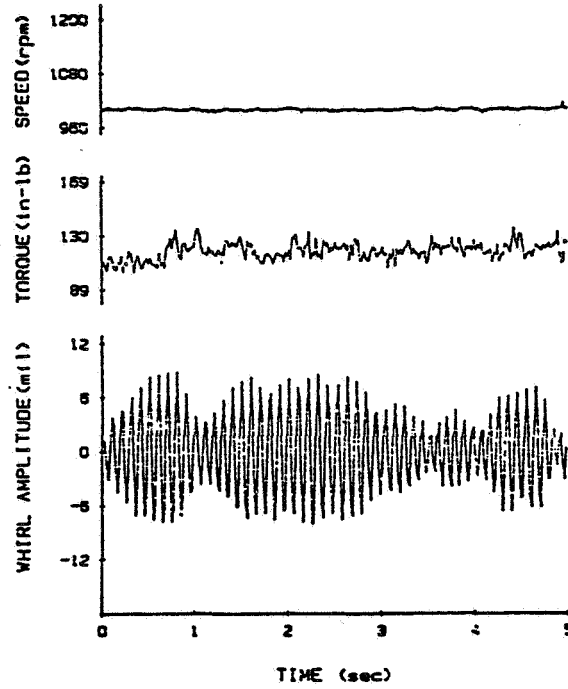


Figure 8. - Time domain data with load torque (2.2 percent damping; 1000 rpm).

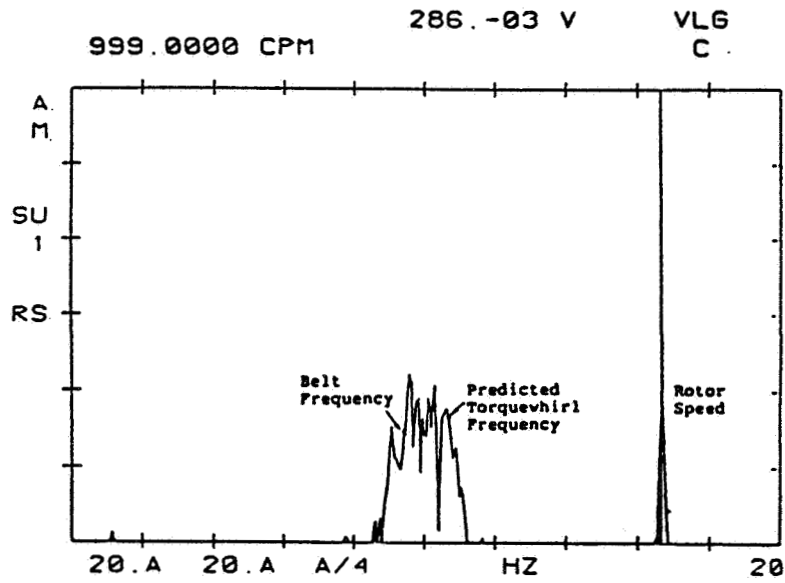


Figure 9. - Frequency domain data with load torque (2.2 percent damping; 1000 rpm).

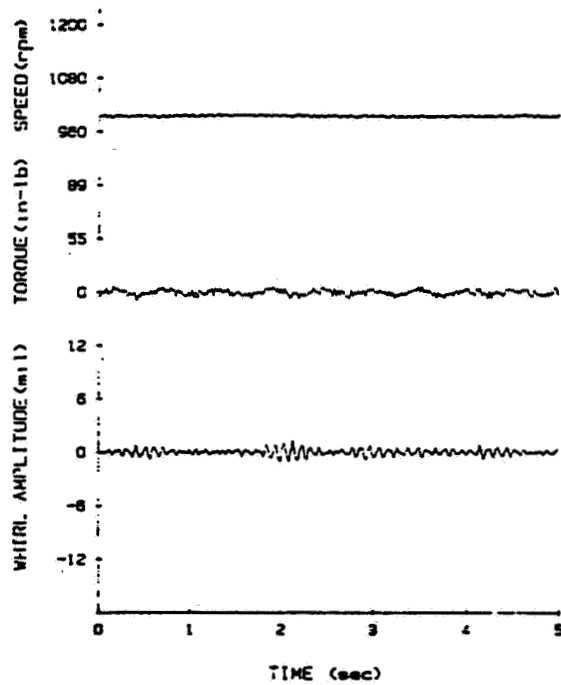


Figure 10. - Time domain data without load torque (5.2 percent damping; 1000 rpm).

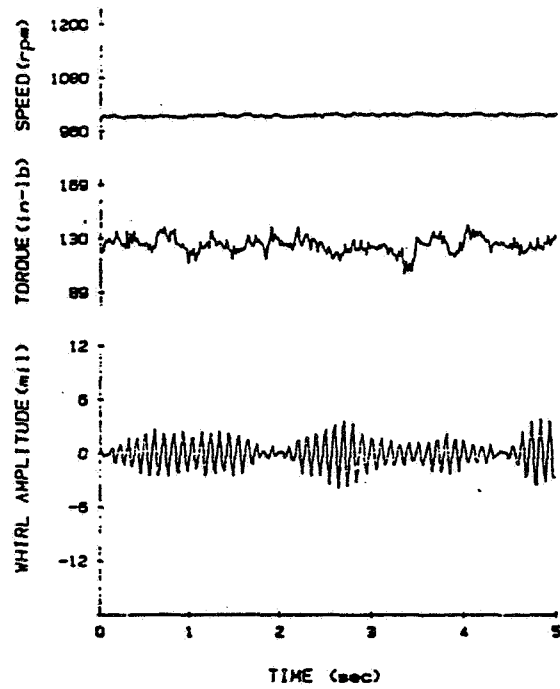


Figure 11. - Time domain data with load torque (5.2 percent damping; 1000 rpm).

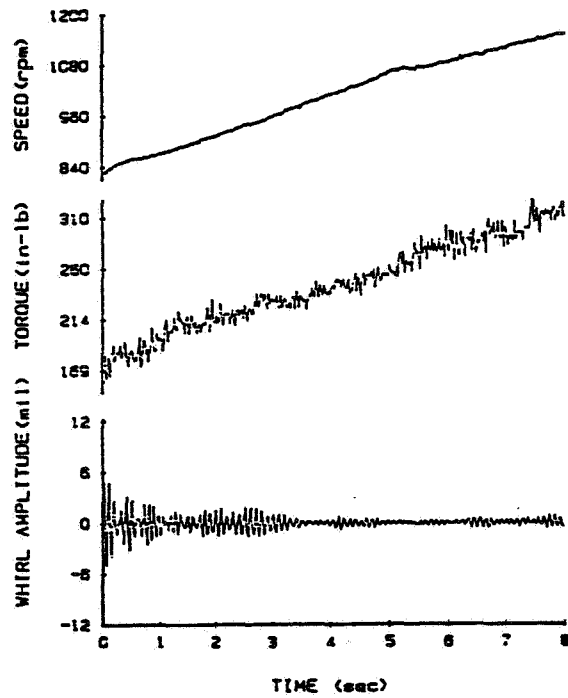


Figure 12. - Time domain data as rotor speed and torque increased continuously.

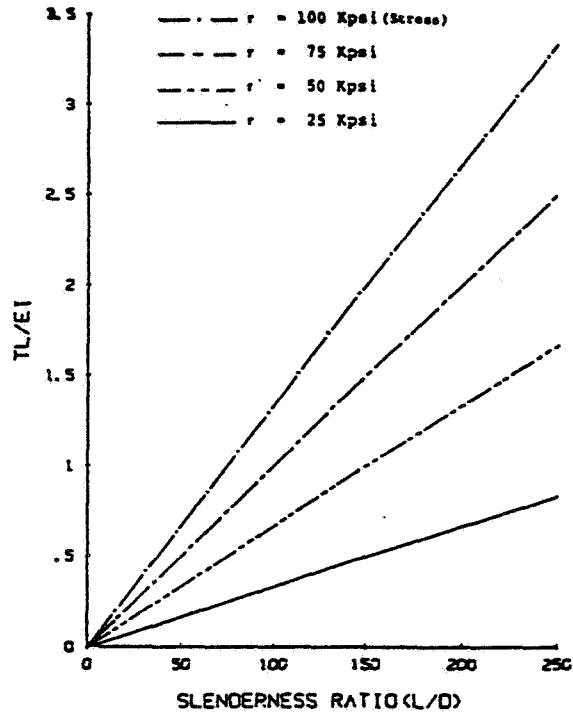
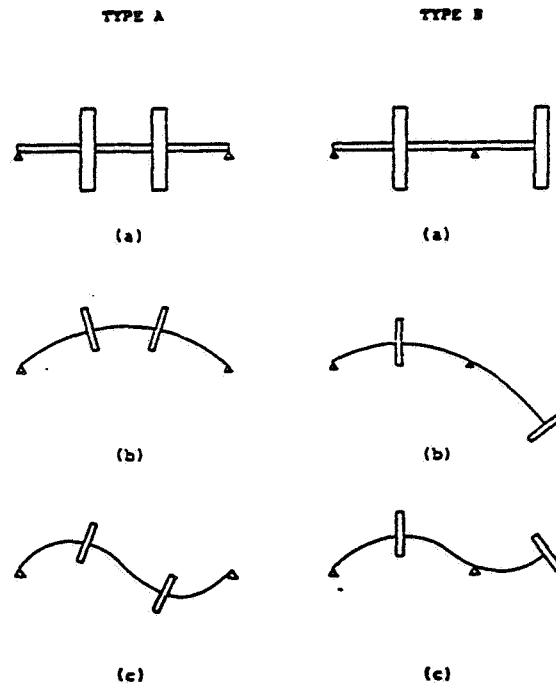


Figure 13. - Dimensionless torque term versus slenderness ratio.



(a) Models. (b) First mode. (c) Second mode.

Figure 14. - Two disk models and their first and second modes.

$l = 60 \text{ in}$ $d = 1 \text{ in}$
 $m_d g = 60 \text{ lb}$ $m_g = 13.3 \text{ lb}$
 $I_c = 0.8 \text{ lb-in-s}^2$ $I_p = 1.6 \text{ lb-in-s}^2$
 $E = 3 \times 10^7 \text{ psi}$ $T = 40000 \text{ in-lb}$
 $K_{xx} = K_{yy} = 5 \times 10^6 \text{ lb/in}$ $N = 7500 \text{ rpm}$

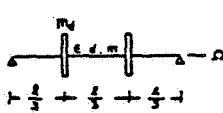
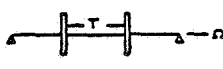
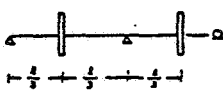
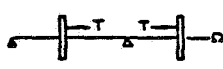
| CASES | Logarithmic Decrement | Frequency (rpm) |
|---|------------------------|-----------------|
| A1  | 0.0 | 312.1B |
| | 0.0 | 376.6F |
| | 0.0 | 1221.4B |
| | 0.0 | 1419.4F |
| A2  | -2.8×10^{-13} | 309.9B |
| | 4.6×10^{-13} | 375.1F |
| | 3.9×10^{-12} | 1217.0B |
| | -1.0×10^{-11} | 1414.5F |
| B1  | 0.0 | 205.9B |
| | 0.0 | 416.8F |
| | 0.0 | 945.4B |
| | 0.0 | 1062.2F |
| B2  | 1.997 | 202.2B |
| | -0.496 | 410.7F |
| | 0.071 | 944.0B |
| | -0.023 | 1058.6F |

Figure 15. - Effect of tangential torque on stability of two-disk rotors.

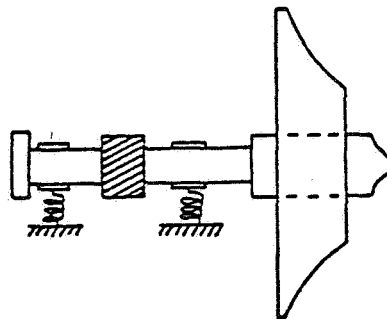
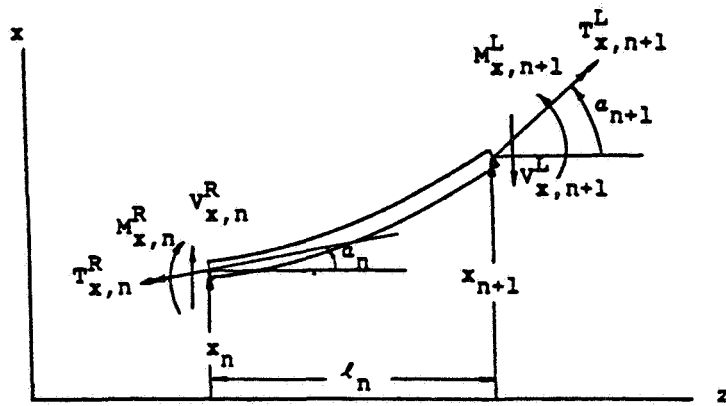
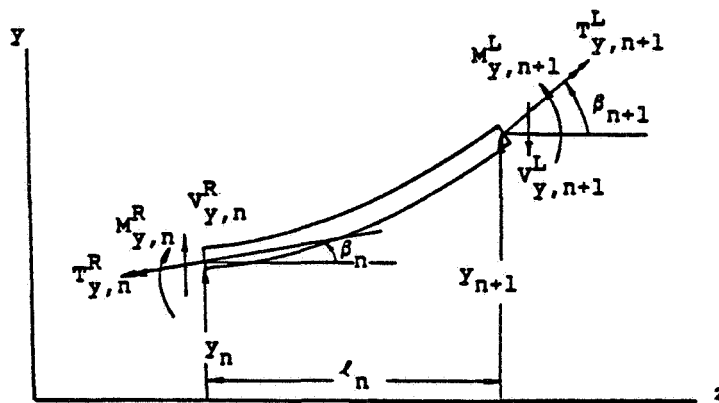


Figure 16. - Single-stage overhung compressor.



(a)



(b)

(a) xz-plane. (b) yz-plane.

Figure 17. - Sign convention for n^{th} shaft section.